A Robust Continuous-Time MPC of a DC-DC Boost Converter Interfaced with a Grid-Connected Photovoltaic System

Rachid Errouissi, *Member, IEEE,* Ahmed Al-Durra, *Senior Member, IEEE,* and S. M. Muyeen, *Senior Member, IEEE,*

***Abstract*—The main function of the dc-dc converter in a grid-connected photovoltaic system, is to regulate the terminal voltage of the PV arrays to ensure delivering the maximum power to the grid. The purpose of this paper is to design and practically implement a robust continuous-time model predictive control (CTMPC) for a dc-dc boost converter, feeding a three-phase inverter of a grid-connected PV system to regulate the PV output voltage. In CTMPC, the system behavior is predicted based on Taylor series expansion, raising concerns about the prediction accuracy in the presence of parametric uncertainty and unknown external disturbances. To overcome this drawback, a disturbance observer is designed and combined with CTMPC to enhance the steady-state performance in the presence of model uncertainty and unknown disturbance such as the PV current, which varies nonlinearly with the operating point. An interesting feature is that the composite controller reduces to a conventional PI controller plus a predictive term that allow to further improve the dynamic performance over the whole operating range. The effectiveness of the proposed controller was tested numerically and validated experimentally with the consideration of the grid-connected PV inverter system and its controller.**

***Index Terms*—Continuous-time model predictive control (CTMPC), dc-dc boost converter, disturbance observer, grid-connected inverter system, photovoltaic system, PI observer, renewable energy.**

I. Introduction

Power electronic converters are essential to ensure efficient and reliable use of the PV power generation in either grid-connected or stand-alone applications. In a grid-connected application, which is the focus of this work, a single/three-phase inverter and a dc-dc converter are usually utilized to interconnect the PV unit to its host grid via a DC-link capacitor. In addition, an input capacitor is normally placed between the dc-dc converter and the PV array to form the PV generator [1]. The main role of the inverter is to regulate the power exchange between the grid and the PV system, so as to comply with the grid code. In such a topology, the active power is controlled by regulating the DC-link voltage [2], while the reactive power is maintained at a specified level, which is mainly dictated by the grid connection requirement [3]. The dc-dc converter is considered to enable extracting the maximum available power from the PV generator by exploring the control capabilities of the switching devices [4]. Among a large number of the existing dc-dc converters, boost converter has become the most commonly used for feeding a grid-tied inverter. The real merit of using a boost converter is its relatively simple topology that is lacking in others dc-dc converters such as a quadrature boost converter, and interleaved boost converter [5], [6]. However, because of its limited efficiency, the boost converter is usually adopted for low power single-phase system, which presents a concern about the DC-link voltage ripples. Such a concern reveals the need for designing an appropriate control of the grid-tied single-phase inverter system, whilst the main focus of this paper is mainly concerned with the control of the boost converter independently of the inverter type. On the other side, a three-phase inverter can guarantee lower DC-link ripples with a classical Proportional-Integral (PI) controller, and it can also be used for some specific low power PV applications such as the household PV installed system. This partially explains why a three-phase grid-tied inverter is chosen, in this research work, to test the performance of the proposed controller for a dc-dc boost converter. However, all the results presented in this paper can be expanded to single-phase grid-connected PV systems.

In the dc-dc boost converter control, a conventional cascaded scheme is widely adopted because of its relatively simple structure, which can ease the controller design and the practical implementation. The cascaded control scheme consists of a fast inner-loop, whose reference value, i.e., the current reference, is provided by a slower outer-loop. The later is designed to control the terminal voltage of the PV array, and its reference value is usually determined by a maximum power point tracking (MPPT) algorithm [7].

In the outer-loop control, a PI controller is well suited to initiate a stable and accurate control, especially when the input capacitor is very big [8]. However, the transient performance may be heavily influenced by the changes in the operating point if the input capacitor is very small due to the so-called dynamic resistance [9]. More recent works have been dedicated to the influence of the dynamic resistance on the PV voltage regulation, including those reported in [10]–[13], and revealed that a PI controller alone may not be an adequate choice to accurately control the boost converter for the whole operating range. Therefore, a PI controller combined with the dynamic resistance estimation might be a judicious solution to guarantee a good dynamic performance independently of the input capacitor size. An early attempt to include the estimate

R. Errouissi, A. Al-Durra, and S. M. Muyeen are with the Petroleum Institute, P.O. Box 2533, Abu Dhabi, United Arab Emirates (e-mails: rerrouissi@pi.ac.ae, aaldurra@pi.ac.ae, and smmuyeen@pi.ac.ae).

This work was supported by "The Petroleum Institute Research Center (PIRC)" Research Grant.

of the dynamic resistance into the PI controller, was through the use of an adaptive PI controller [12]. The basis for such a controller relies on estimating the dynamic resistance to continuously adjust the controller parameters, so as to cancel the undesired effect caused by the PV current variation. In that work, the proposed controller was applied to a single-phase system, and the inherent current and voltage ripples were used to determine the dynamic resistance. However, this approach breeds other problems such as the limited estimation accuracy in the presence of the measurement noise. Another drawback of that method is its limited applicability to a single-phase system. A recent attempt to preserve the nominal tracking performance over the entire operating range was through the use of a disturbance observer-based control (DOBC) [13]. In that work, good performances were obtained, but only a stand-alone application was considered, and no realistic scenarios were performed under grid-connected PV system.

In light of the aforementioned problems related to the PI controller, this paper proposes a design methodology to derive a predictive PI controller for a dc-dc boost converter feeding a grid-tied inverter. The whole derivation is based on combining a Model Predictive Control (MPC) and a Disturbance Observer (DO). The MPC is essentially an optimal control that minimizes a quadratic cost function consisting of the difference between the system output and the trajectory to be tracked over a finite time horizon. The proposed MPC, known as Continuous-Time MPC (CTMPC), uses Taylor series expansion to predict the system behavior by considering the nominal model [14]–[16]. The disturbance observer is introduced to estimate the uncertain part, not considered in the nominal model, to improve the prediction accuracy [17]–[19]. In this work, the major role of the disturbance observer is to estimate the PV current instead of the dynamic resistance. It turns out that the composite controller, consisting of CTMPC and DO, reduces to a PI controller plus a predictive term that has the role of improving the tracking performance for a smooth reference signal. The design process and the additional predictive part represent the essential difference between the proposed method and the existing adaptive PI controllers. An adequate choice of the reference signal permits to have a good dynamic response by exploring the tracking performance capabilities of the predictive controller, while the integral action eliminates the steady-state error. Another advantage lies in the estimation of the PV current instead of the dynamic resistance. Such an estimation can be directly used for other algorithms, such as MPPT technique, which avoids the need for additional filter for the current measurement. Similar design process is recently adopted in [20] to develop an accurate control of a solar energy conversion system consisting of a dc-dc boost converter and a grid-tied inverter. However, that work focuses only on the control of a grid-tied inverter without treating the control of the dc-dc boost converter, and only a PI controller is used to regulate the PV output voltage. Another difference is that the proposed disturbance observer reduces to a PI controller in this work, while the work presented in [20] considers the integration of the system model to estimate the lumped disturbances due to the existence of unmatched disturbances, raising concern about the relative complexity of real-time implementation.

In the inner-loop control, several approaches have been proposed to achieve a fast transient response, including the finite-control-set model predictive control (FCS-MPC) [21], sliding mode control (SMC) [22], [23], PI controller [24], etc. In this paper, a PI controller is derived for the inner-loop control using the same design process as for the outer-loop. Finally, the effectiveness of the proposed controller was validated with the consideration of a grid-connected three-phase inverter, so as to take into account the real dynamics of the whole system. PI controllers are designed to control the three-phase grid-tied inverter.

II. System Modeling

Figure 1 shows the schematic of a dc-dc boost converter tied to the ac bus via a DC-link capacitor C, a three-phase inverter, and a line filter composed of an inductance L and a resistance R. The DC-link voltage v_{dc} is kept constant by controlling the switching devices $S_{\{1,6\}}$. The main focus of this work is to regulate the PV output voltage v_0 through the switching actions of the semiconductor device S_b. Here, C_b and L_b, represent the input capacitor and the boost inductor, respectively. For the boost converter, the measurable variables are the inductor current i_L and the PV voltage v_0. The voltage v_{dc} is seen as a known disturbance, whereas the current i_p is considered as an unknown disturbance that needs to be estimated and compensated in the control law.

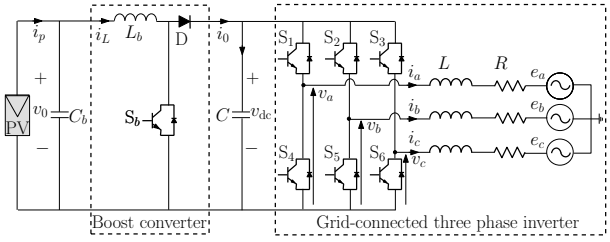

Fig. 1. Schematic diagram of a PV three-phase conversion system.

Assuming that the converter operates in a continuous conduction mode, then, the dynamics of the boost converter depicted in Fig. 1 can be described by the following set of differential equations

$$\begin{cases} \dfrac{di_L}{dt} = \dfrac{v_0}{L_b} - \dfrac{v_{dc}}{L_b} + \dfrac{v_{dc}}{L_b} d \\ \dfrac{dv_0}{dt} = -\dfrac{i_L}{C_b} + \dfrac{i_p}{C_b} \end{cases} \tag{1}$$

where d represent the duty-cycle control. In the cascaded scheme, the inner current control loop provides the duty-cycle d, which is realized by means of a fixed frequency PWM. Making use of (1), the current controller can be designed based on the linear model of the current equation given by

$$\frac{di_L}{dt} = A_i i_L + B_i u_i + F_i b_i, \quad u_i = (d-1)\,. \tag{2}$$

where

$$A_i = 0,\ B_i = \frac{v_{dc}}{L_b},\ F_i = \frac{1}{L_b},\ b_i = v_0 + \delta_i \tag{3}$$

The term δ_i is added to the model to represent the lumped disturbances caused by model uncertainty. In the outer voltage loop, the current i_L is treated as a control input. Thus, the current reference, for the inner-loop, can be determined from the outer-loop voltage control based on the following linear model

$$\frac{dv_0}{dt} = A_v v_0 + B_v u_v + F_v b_v, \quad u_v = i_L. \tag{4}$$

where

$$A_v = 0,\ B_v = -\frac{1}{C_b},\ F_v = \frac{1}{C_b},\ b_v = i_p + \delta_v \tag{5}$$

The term δ_v represents parameter variations and external disturbances. In order to simplify the controller design, it is assumed that

$$\lim_{t\to\infty} \dot{\delta}_i(t) = 0, \qquad \lim_{t\to\infty} \dot{\delta}_v(t) = 0 \tag{6}$$

III. Robust Continuous-Time Model Predictive Control (CTMPC)

A. Baseline Controller: Formulation of CTMPC

Consider a mathematical model for a single-input-single-output (SISO) disturbed linear system

$$\dot{y} = Ay + Bu + Fb \tag{7}$$

where $u \in \mathbb{R}$, $y \in \mathbb{R}$, and $b \in \mathbb{R}$, are the input, the output, and the disturbance, respectively. The continuous-time MPC is essentially an optimal control that results from minimizing a quadratic cost function defined by

$$\Im = \left[e\left(t+T_r\right)\right]^2 = \left[y_r\left(t+T_r\right) - y\left(t+T_r\right)\right]^2 \tag{8}$$

where, y_r represents the output reference, $e(t)$ is the tracking error, and T_r is known as predictive time. In the continuous-time MPC formulation, the control input is not usually included in the cost function to simplify the stability analysis. In such conditions, the control effort can be restricted by tuning the predictive time T_r or/and limiting the set-point changes. The optimal control is derived based on the optimality condition given by

$$\frac{d\Im}{du} = 0 \tag{9}$$

Following [18], the design methodology of a continuous-time MPC is based on approximating the future tracking error $e(t+T_r)$ with the use of Taylor series expansion up to $(\rho+r)^{th}$ order, with r denotes the control order and ρ is the relative degree of the system. The main role of the control order is to ensure the stability of the closed-loop system for systems having high relative degree [25]. However, for the system under investigation, it is clear that the relative degree is equal to 1 for both loops. That is why, the control order r is set equal to be zero in this work. Hence, an approximate of $e(t+T_r)$ is given by

$$e\left(t+T_r\right) = e\left(t\right) + T_r \dot{e}\left(t\right) \tag{10}$$

Making use of (7), from the definition of the relative degree ρ, it follows that

$$\dot{e}\left(t\right) = \dot{y}_r\left(t\right) - \dot{y} = \dot{y}_r\left(t\right) - Ay - Bu - Fb \tag{11}$$

Hence, (10) can be simplified as

$$e\left(t+T_r\right) = \Pi(T_r)\left(H\left(y\right) - Gu - Mb\right) \tag{12}$$

where

$$\Pi = \begin{bmatrix} 1 & T_r \end{bmatrix}, \quad H\left(y\right) = \begin{bmatrix} e\left(t\right) & \dot{y}_r\left(t\right) - Ay \end{bmatrix}^T \tag{13}$$

The column matrices G and M are given by

$$G = \begin{bmatrix} 0 \\ B \end{bmatrix}, \quad M = \begin{bmatrix} 0 \\ F \end{bmatrix} \tag{14}$$

Invoking (13)–(14), and replacing $e(t+T_r)$ in (8) by its expression given by (12), the approximate cost function $\Im$ can be expressed as follows

$$\Im = \left(H\left(y\right) - Gu - Mb\right)^T \Upsilon\left(T_r\right)\left(H\left(y\right) - Gu - Mb\right) \tag{15}$$

where $\Upsilon\left(T_r\right)$ is a 2×2 matrix and is determined as follows

$$\Upsilon\left(T_r\right) = \Pi^T\left(T_r\right)\Pi\left(T_r\right) \tag{16}$$

The derivative of the cost function with respect to the control input is given by

$$\frac{d\Im}{du} = -B\begin{bmatrix} \Upsilon_1 & \Upsilon_2 \end{bmatrix} H\left(y\right) + B\Upsilon_2 Bu + B\Upsilon_2 Fb \tag{17}$$

where $\Upsilon_1 = \Upsilon_{2,1}$, and $\Upsilon_2 = \Upsilon_{2,2}$. Thus, considering the matrix $\Upsilon(T_r)$, it can be shown that

$$\Upsilon_1 = T_r, \quad \Upsilon_2 = T_r^2 \tag{18}$$

Making use of $\frac{d\Im}{du} = 0$, the optimal control is given by

$$\begin{aligned} u\left(t\right) =& B^{-1}\left(\Upsilon_2^{-1}\begin{bmatrix} \Upsilon_1 & \Upsilon_2 \end{bmatrix} H\left(y\right) - \Upsilon_2^{-1}\Upsilon_2 Fb\right) \\ =& B^{-1}\left(\begin{bmatrix} K & 1 \end{bmatrix} H\left(y\right) - Fb\right) \end{aligned} \tag{19}$$

where the controller gain K is expressed as follows

$$K = \frac{1}{T_r} \tag{20}$$

Substituting (19) in (11) gives the closed-loop system error equation as follows

$$\dot{e} + Ke = 0 \tag{21}$$

Therefore, since the predictive time is positive, it is clear that the closed-loop system, under the continuous-time MPC, is asymptotically stable. For real-time implementation, the disturbance is not always available for measurement. For the purpose of making the proposed controller more convenient for practical implementation, the continuous-time MPC can be modified as

$$\begin{aligned} u\left(t\right) &= B^{-1}\left(\begin{bmatrix} K & 1 \end{bmatrix} H\left(y\right) - F\hat{b}\right) \\ &= B^{-1}\left(Ke\left(t\right) + \dot{y}_r - Ay - F\hat{b}\right) \end{aligned} \tag{22}$$

where $\hat{b}$ is an estimate of the real disturbance b.

B. Composite Controller: CTMPC and a Disturbance Observer

Considering the measurement of the output y, an observer can be derived to estimate the disturbance as follows [26],

$$\dot{\hat{b}} = \mu \left(\dot{y} - Ay - Bu - F\hat{b} \right) \tag{23}$$

where μ is the observer gain. Combining (7) with (23), gives the dynamics of the disturbance observer as follows

$$\dot{e}_b = -\mu F e_b - \dot{b} \tag{24}$$

where $e_b = \hat{b} - b$ is the disturbance estimation error. It is evident that the disturbance observer can be made stable by choosing the parameter μ so as to have $\mu F > 0$. This means that the estimation error can be made bounded and its bound depends on $\dot{b}$. Hence, with the assumption that $\lim_{t \to \infty} \dot{b} = 0$, it is clear that the observer converges to the actual disturbance as $t \to \infty$. According to (24), a large observer gain μ results in a fast disturbance estimation, but it may magnify the measurement noises. Hence, attention should be given when selecting the observer gain for practical implementation. The major drawback of the observer (23) is that it includes the time derivative of the output. To tackle the need for $\dot{y}$, the disturbance observer can be further simplified by substituting the control law (22) into (23). In doing so, we obtain

$$\dot{\hat{b}} = -\mu K e(t) - \mu \dot{e}(t) \tag{25}$$

By integrating the above equation, one can simplify the disturbance observer as follows

$$\hat{b}(t) = -\mu K \int_0^t e(\tau)\, d\tau - \mu e(t) + \mu e(0) + \hat{b}(0) \tag{26}$$

Hence, as pointed out in [18], selecting $\hat{b}(0) = -\mu e(0)$ allows recovering approximately the nominal performance, defined by (21), in the absence of disturbances. For instance, substituting (22) into (11) with the consideration of (26) gives the output tracking error dynamics as follows

$$\dot{e}(t) + (K + F\mu) e(t) + F\mu K \int_0^t e(\tau)\, d\tau = -Fb + F\xi(0) \tag{27}$$

where $\xi(0) = \hat{b}(0) + \mu e(0)$. Therefore, by neglecting the disturbance variation, the reference-to-output transfer function $P(s)$, for a constant set-point, can be expressed by

$$\mathrm{P}(s) = \frac{(K + F\mu)\, s + F\mu K}{s^2 + (K + F\mu)\, s + F\mu K} \tag{28}$$

The poles associated with (28) are $s_1 = -K$ and $s_2 = -F\mu$. This implies that the closed-loop system is asymptotically stable, since the predictive time T_r is positive and the observer gain μ satisfies $\mu F > 0$, as mentioned above. According to (28), it is clear that the disturbance observer has also an impact on the dynamic performance.

Remark 1: To facilitate the design process, the predictive time T_r can be considered as the first design parameter, which must be selected as small as possible, since the control methodology is based on Taylor series expansion. For power converter applications, the predictive time is mainly decided by the switching frequency [27], which dictates the nominal performance specification of the settling time defined by (21). The observer gain is selected to correspond to the desired settling time under the composite controller by considering the transfer function (28).

Remark 2: It it noticed that if the disturbance b is composed of a measurable variable b_m and an unknown component b_u, with $b = b_m + b_u$, the composite controller can be modified as

$$u(t) = B^{-1} \left(Ke(t) + \dot{y}_r - Ay - Fb_m - F\hat{b}_u \right) \tag{29}$$

where $\hat{b}_u$ is simply computed by the PI observer given by (26). Now, assuming that $\hat{b}_u(0) = -\mu e(0)$, and substituting (26) into (29) gives the predictive PI controller as follows

$$u(t) = P_b e(t) + I_b \int_0^t e(\tau)\, d\tau + N_b(t) \tag{30}$$

where $P_b = B^{-1}(K + F\mu)$, and $I_b = B^{-1} FK\mu$ are the proportional and the integral gains of the PI controller, respectively. The predictive term $N_b(t) = B^{-1}(\dot{y}_r - Ay - Fb_m)$ has the role of predicting the error between the system output y and the trajectory to be tracked y_r. Such a term is not usually considered in the classical PI controller, which makes the proposed controller superior in terms of the tracking performance, particularly, when dealing with a smooth reference.

C. Application to the Boost Converter

The composite controller, consisting of a continuous-time MPC and a disturbance observer, is applied to the dc-dc boost converter by means of the conventional cascaded scheme. For the inner-loop, the composite controller is applied to the current dynamics (2) to determine the duty-cycle $d = (u_i + 1)$ minimizing the cost function (8), with $y = i_L$, and $y_r = i_{Lref}$, where i_{Lref} is the current reference. Invoking (30), the inner-loop controller can be expressed as

$$u_i = \frac{L}{v_{dc}} \left(\left(K_i + \frac{\mu_i}{L_b} \right) e_i(t) + \frac{\mu_i K_i}{L_b} \int_0^t e_i(\tau)\, d\tau - \frac{1}{L_b} v_0 \right) \tag{31}$$

where $e_i = i_{Lref} - i_L$ is the current tracking error. Under a cascaded structure, the current reference i_{Lref} is generated by the outer-loop control. This can be accomplished by applying the predictive PI controller (30) to the equation (4) to find the optimal input $u_v = i_{Lref}$ minimizing the cost function (8), with $y = v_0$ and $y_r = v_{0ref}$, where v_{0ref} is the desired voltage reference. In doing so, we get

$$u_v = -C_b \left(\left(K_v + \frac{\mu_v}{C_b} \right) e_v(t) + \frac{\mu_v K_v}{C_b} \int_0^t e_v(\tau)\, d\tau + \dot{v}_{0ref} \right) \tag{32}$$

where $e_v = v_{0ref} - v_0$ is the PV voltage tracking error.

Remark 3: It should be noted that the time derivative of the current is not included in the current loop control to avoid magnification of the measurement noise, since the current

reference $i_{Lref} = u_v$ is based on the voltage measurement. As a result, the composite controller for the inner-loop reduces to a PI controller with a feed-forward term that compensates the variation of both the DC-link and the PV voltages. Note that the value of V_{dc} is updated in the inner-loop control.

Remark 4: For the voltage regulation, the composite controller includes the time derivative of the reference, which allows improving the tracking performance in comparison to a conventional PI controller. Therefore, a filtered voltage reference can be used, instead of a step input, to take advantage of the tracking capability of the proposed controlled, while at the same time, to limit the inductor current during the transient.

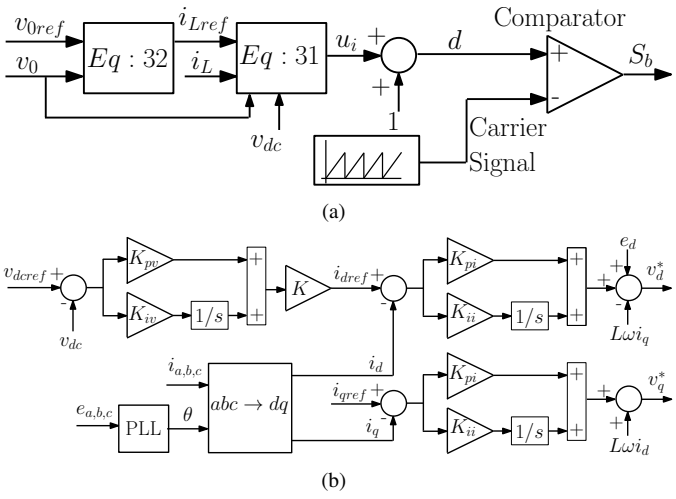

Fig. 2. Control schemes for (a) dc-dc converter (b) grid-tied inverter, with $K = \frac{2v_{dcref}}{3e_d}$, and $K_{pi} = 14.2419$, $K_{ii} = 7.4570\times10^3$, $K_{pv} = 0.1403$, and $K_{iv} = 7.0133$.

IV. Computer Simulations

A. Control Loop Diagram

Figure 2 shows the control block diagram for both the dc-dc boost converter and the three-phase grid-connected inverter. The control scheme for a three-phase grid-connected inverter, reported in the literature, has traditionally a cascaded structure, consisting of PI controllers. The outer-loop regulates the DC-link voltage by considering the d-axis current i_d as a control input, while the inner-loop uses the voltage components v_d and v_q to control the currents i_d and i_q. The voltage commands v_d^* and v_q^* are then converted to three-phase voltage commands v_a^*, v_b^*, and v_c^*, which can be realized with PWM techniques. The q-axis current i_q is generally maintained equal to zero to achieve unity power factor operation. The components in the synchronous rotational frame $(d,\ q)$ are obtained via $abc - dq$ transformation with the use of a phase-locked loop (PLL) algorithm to generate the reference angle so as to maintain $e_q = 0$, where e_q denotes the q-axis grid voltage [28]. This means that the d-axis grid voltage e_d will be aligned with the grid voltage vector. Following [29], the coefficients K_{pi} and K_{ii} of the PI controller for the inner-loop can be designed with $K_{pi} = 2\zeta L\omega_{ni} - R$, and $K_{ii} = L\omega_{ni}^2$, respectively, while those for the outer-loop can be determined with $K_{pv} = 2\zeta C\omega_{nv}$, and $K_{iv} = C\omega_{nv}^2$, respectively, where ζ denotes the damping ratio and $\omega_{ni,v}$ represents the natural angular frequency. The typical value of ζ is equal to $\frac{1}{\sqrt{2}}$, while $\omega_{ni,v}$ can be selected according to the desired settling time approximated by $\frac{4}{\zeta\omega_{ni,v}}$, with the consideration of the switching frequency [30]. It is noticed that, in the cascaded scheme, the outer-loop should be designed to have slower response than that of the inner-loop. To demonstrate the effectiveness of the proposed approach, simulation tests are carried out using MATLAB/SIMULINK with the use of a single diode PV panel model, developed in [31]. Under standard conditions, the PV panel can operate at a maximum power point (MPP) of 1 kW, and its *I–V* characteristic curve is plotted in Fig. 3. The switching frequency for the dc-dc boost converter is selected to be f_{sc} = 12.5 kHz, while that for the three-phase inverter is set to be f_{si} = 6.25 kHz. The simulation tests were performed with a control period of 80 μsec. The time step for the complete developed model is set equal to 1 μsec.

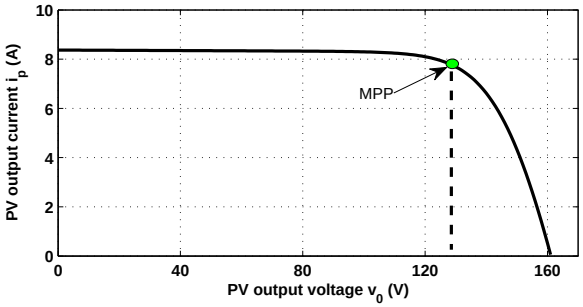

Fig. 3. Characteristic *I–V* curve of the PV array under standard conditions, with $I_{MPP} = 7.75$ A, $V_{MPP} = 129$ V, and $P_{MPP} = 1$ kW.

The parameters of the proposed controller for the dc-dc boost converter can be determined based on the nominal specifications of the settling time $t_{sc} \approx 4T_r$, defined by (21), by considering the minimum switching frequency f_{sc} of the semiconductor device. That is, the predictive time T_r, which is the first design consideration, for the inner-loop and the outer-loop is set to be 0.2 ms and 2 ms, respectively, to achieve a fast and stable control under cascaded structure. For the observer gains, selecting μ_i = 0.1 modifies the settling time of the closed-loop current control to be equal to nine times the switching period $T_{sc} = 1/f_{sc}$, which is fast enough [27]. The observer gain μ_v should be chosen as large as possible, while maintaining the response of the voltage control slower than that of the current control to ensure the stability of the cascaded control scheme. Thereby, the observer gain μ_v is set to be 0.5, so that the settling time of the outer-loop becomes equal to five times that of the inner-loop. Moreover, the voltage reference is realized by a first-order linear filter, with a time constant equal to T_r = 2 ms, to avoid overshoot that can be caused by the integral action in response to a step input. Such a strategy allows limiting the inductor current during the transient, and eliminating the steady-state error without scarifying the nominal tracking performance. The parameter values of the complete developed system are given in the Appendix.

B. Tracking Performance Under Maximal Power Point

First test was concerned with the reference tracking performance evaluation with a step change in the PV voltage reference from 158 to 130 V. The PV voltage of 130 V has been selected to extract the maximum power from the PV panel. Such a test is equivalent to a change in the active power P delivered to the grid, with $P : 0 \rightarrow 1kW$.

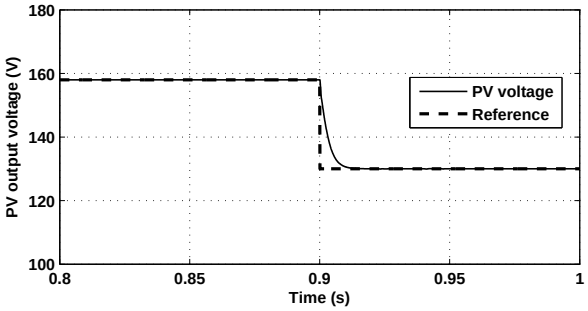

Fig. 4. PV output voltage response.

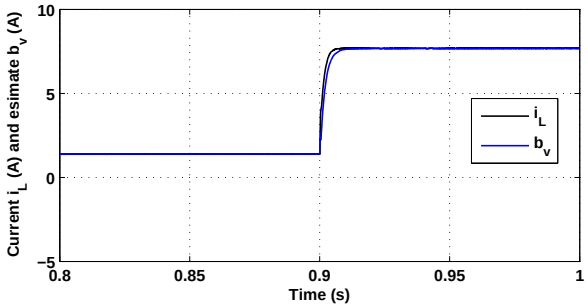

(a) Inductor current and the disturbance estimation.

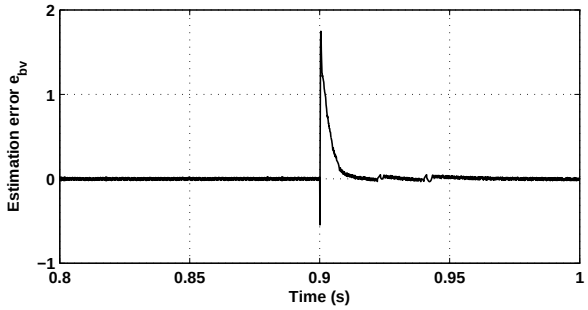

(b) Estimation error $e_{bv} = i_L - b_v$

Fig. 5. Inductor current response to a step change in v_0.

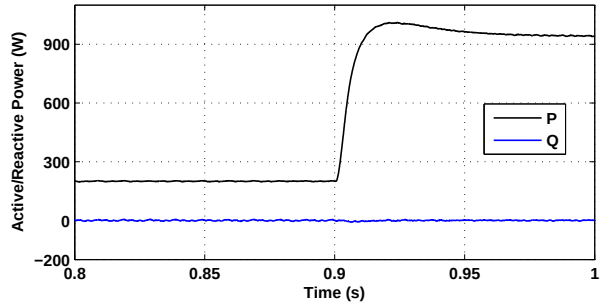

Fig. 6. Active and reactive powers delivered to the grid in response to a step change in v_0

Figure. 4 shows that the PV output voltage tracked its reference with zero steady-state error in spite of unknown PV current i_p, which varies nonlinearly with the operating point. As can be seen in Fig. 5, the estimate b_v followed the inductor current i_L with an error which tends to zero as time goes to infinity, indicating that the disturbance observer is asymptotically stable, since the current i_L is equal to the unknown component i_p in the steady-state regime. As illustrated in Fig. 6, the reactive power Q is maintained equal to zero, while the active power P follows its command of 1 kW with a steady-state error resulting from the inverter losses.

C. Tracking Performance Under a Time-Varying Reference

This test was performed with step changes in the PV output voltage to verify the effectiveness of the proposed controller throughout the whole operating range. That is, downward steps of the PV voltage were realized from 158V, near to the open-circuit voltage, to 120 V, below the MPP voltage, as $v_{0ref} = 158 \rightarrow 145 \rightarrow 135 \rightarrow 120$ V. Also, upward steps were realized as $v_{0ref} = 120 \rightarrow 135 \rightarrow 145 \rightarrow 158$ V.

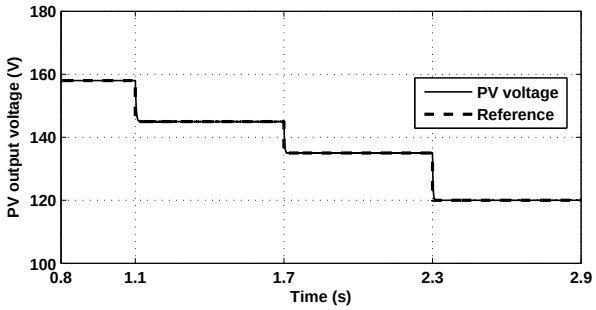

(a) PV output voltage response

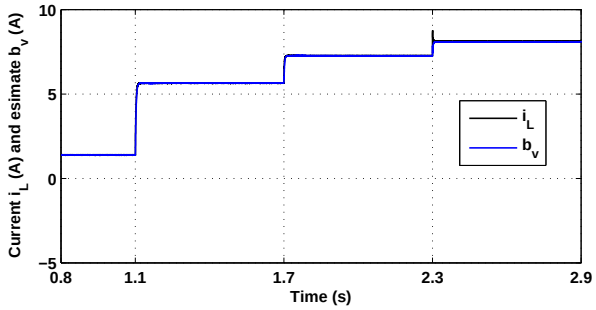

(b) Inductor current and the disturbance estimation b_v

Fig. 7. Tracking performance with downward steps of v_0.

According to Figs. 7(a) and 8(a), the proposed controller allows achieving good transient and steady-state performances independently of the operating points. More interestingly, similar dynamic performance can be observed over the entire operating range. The inductor current i_L, shown in Figs. 7(b) and 8(b), exhibits a good dynamic performance without a significant overshoot as the PV voltage changed due to the filtered PV voltage reference. Similarly to the previous test, the estimate b_v closely followed the inductor current i_L.

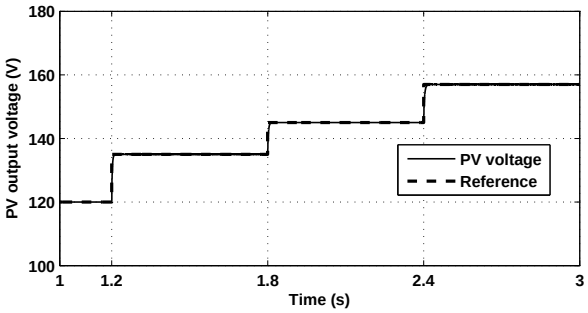

(a) PV output voltage response

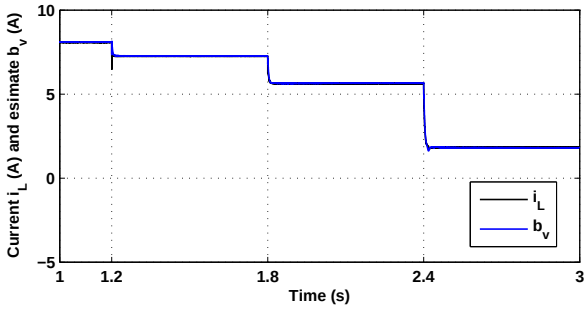

(b) Inductor current and the disturbance estimation b_v

Fig. 8. Tracking performance with upward steps of v_0.

V. Experimental Results

A. Experimental Setup

Experimental tests were conducted to validate the proposed controller with the consideration of realistic scenarios by connecting the output of the dc-dc converter to a grid-connected inverter as shown in Fig. 9.

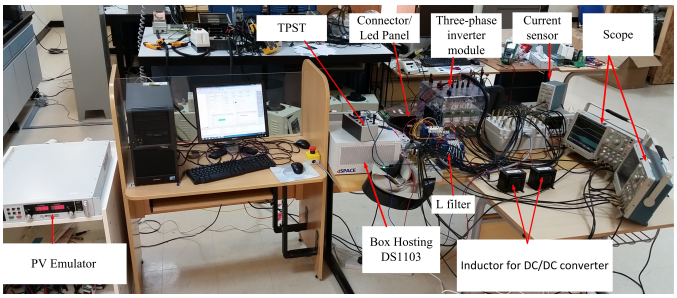

Fig. 9. Laboratory setup for testing the proposed controller

The experimental setup consists of a PV emulator including the input capacitor C_b, a dc-dc boost converter, a DC-link capacitor, a three-phase inverter and an L type filter to smooth the current injected into the grid. A XR160-12 power supply module, manufactured by Magna-Power Electronics, was used to produce the PV power according to the I-V characteristic shown in Fig 3. Semiteach power electronics module (AN-8005), manufactured by Semikron, was utilized to construct a six-pulse IGBT inverter and a dc-dc converter. The PI controller for the grid-side inverter and the predictive controller for the dc-dc converter were realized using the dSPACE ds1103 DSP board. The hardware realization employs the previously given values of the controller parameters, the switching frequencies, and the control period. However, in practice, it has found that the PV output voltage regulation, with $\mu_v = 0.5$, is unstable. Such a difference between the simulation and experimental test is possibly explained by the fact that $\mu_v = 0.5$ causes the settling time of the voltage control to approach that of the current control, which certainly affects the stability of the cascaded control scheme. To address such a concern, the observer gain μ_v is set to be 0.1, so that the settling time of the outer-loop is equal to twelve times that of the inner-loop.

B. Tracking Performance Under Maximal Power Point

This experimental test was performed to validate the first simulation results, where a step change in the PV voltage was applied to the dc-dc converter to ensure delivering the maximum power to the grid. The experimental results are presented in Figs. 10 and 11, showing that the PV voltage regulation performance is almost similar to that obtained with simulation test. However, it can be observed that the inductor current response is evidently slower than that obtained with the simulation test. Such a difference between simulation and experimental results can be possibly explained by the inherent dynamics of the PV emulator to a rapid change in PV voltage.

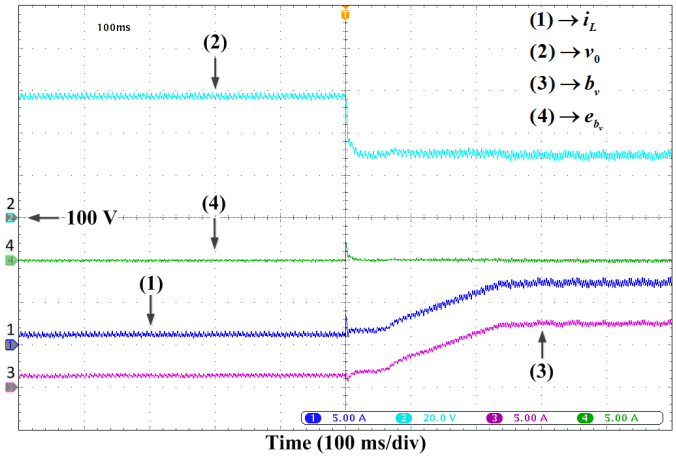

Fig. 10. Boost converter's response under a step input of PV voltage: v_0(20 V/div), i_L(5 A/div), b_v(5 A/div), and e_{b_v}(5 A/div).

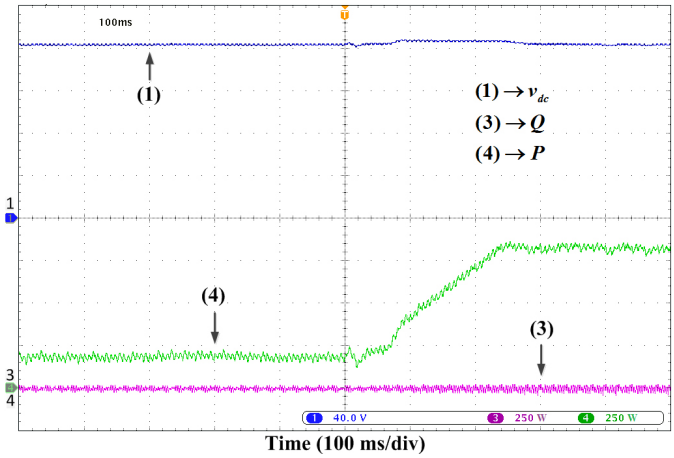

Fig. 11. DC-link voltage and active/reactive power delivered to the grid under a step input of PV voltage: v_{dc}(40 V/div), P(250 W/div), and Q(250 W/div).

Also, it can be seen that the estimate b_v tracked accurately the inductor current i_L and the estimation error e_{b_v} converges to zero at the steady-state regime. For the grid-tied inverter control, it is clear that that the DC-link voltage and the reactive power Q are well controlled. Here, P represents the active transferred to the grid. The unity power factor operation is guaranteed as shown in Fig. 12. It is noted that the modulating signals m_a^*, m_b^*, and m_c^* are generated using third harmonic injection technique, so as to to prevent over-modulation problem.

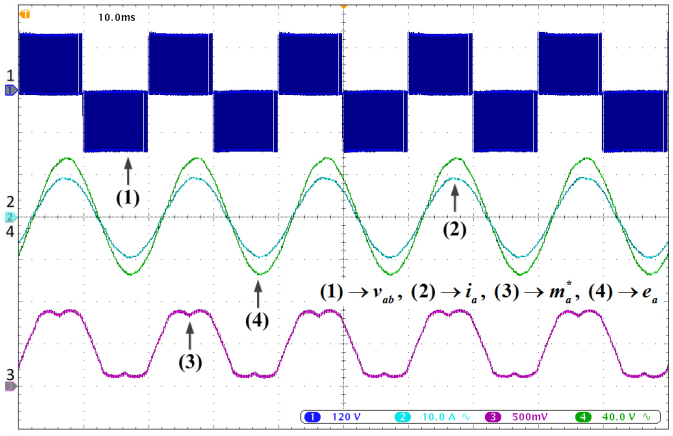

Fig. 12. Grid current i_a, grid voltage e_a, the voltage v_{ab} at the output of the inverter, and the reference of the modulating signal m_a^* using the third harmonic injection technique: i_a(10 A/div), e_a(40 V/div), v_{ab}(120 V/div), and m_a^*(0.5 V/div).

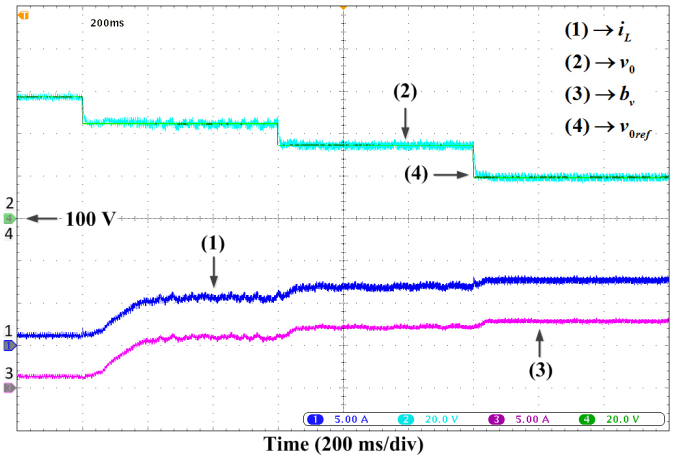

Fig. 13. Performance evaluation under downward steps of v_0: v_0(20 V/div), i_L(5 A/div), and b_v(5 A/div).

C. Tracking Performance Under Different Operating Points

This experiment was performed to experimentally test the tracking performance with the continuous-time MPC in response to downward and upward steps of the PV voltage reference over the entire operating range. Experimental results shown in Figs. 13 and 14 , confirmed the simulation results for good transient and steady-state performances throughout the whole operating range. Also, it can be seen that the disturbance observer responds well, with the estimate b_v following accurately the inductor current i_L. Similarly to the previous test, the inductor current response is slow in comparison with the simulation test because of the limited dynamics of the PV emulator.

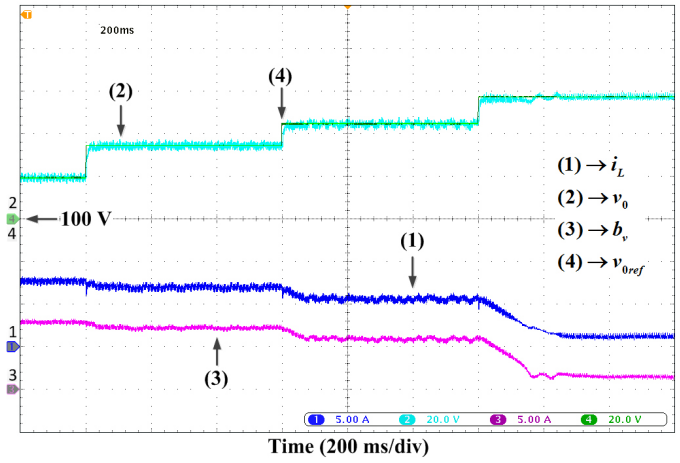

Fig. 14. Performance evaluation under upward steps of v_0: v_0(20 V/div), i_L(5 A/div), and b_v(5 A/div).

D. Comparison Between CTMPC and the PI Controller

This experiment is concerned with the performance comparison of the proposed approach and the classical PI controller, for the PV output voltage regulation, while maintaining the same inner-loop control to have a fair comparison. Following [23], the coefficients P_b and I_b of the PI controller can be designed as $P_b = 2\zeta C_b \omega_{nb}$, and $I_b = C_b \omega_{nb}^2$, with $\zeta = 0.7$. The natural angular frequency ω_{nb} is set to be equal to 661 rad/s, so that the resulting settling time is the same as that obtained with CTMPC, i.e., equal to twelve times that of the inner-loop. Such a design process enables us to perform a fair comparison.

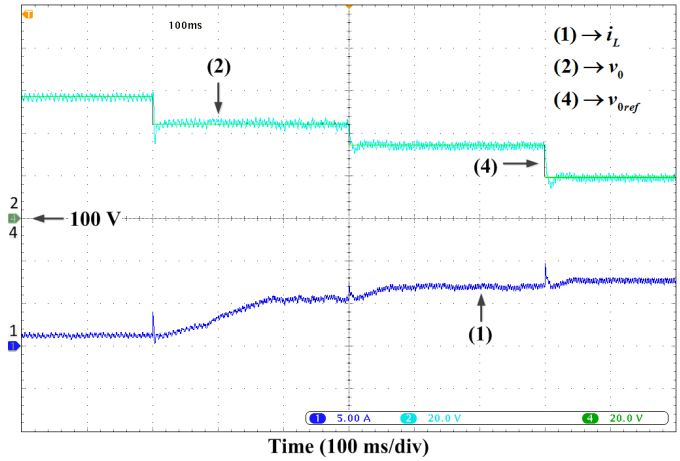

Fig. 15. Voltage and current waveforms in response to upward steps of v_0 under PI controller, and with nominal value of C_b: v_0(20 V/div), i_L(5 A/div).

Fig. 15 gives the voltage and current waveforms in response to downward steps of the PV output voltage under the PI controller, designed with the nominal value of C_b. Figs. 16 and 17 compare the performance of the proposed CTMPC with the PI controller under model uncertainty. More specifically,

the value of C_b is set incorrectly in the controllers, and it is chosen to be equal to 25% of its nominal value. As seen, under nominal value of C_b, the PI controller allows achieving a good transient response of the boost converter over the whole operating range, but a degraded performance is observed under model uncertainty as shown in Fig. 16. As illustrated in Fig. 17, the proposed design process is proved to be effective regarding model uncertainty in comparison with the classical PI controller design.

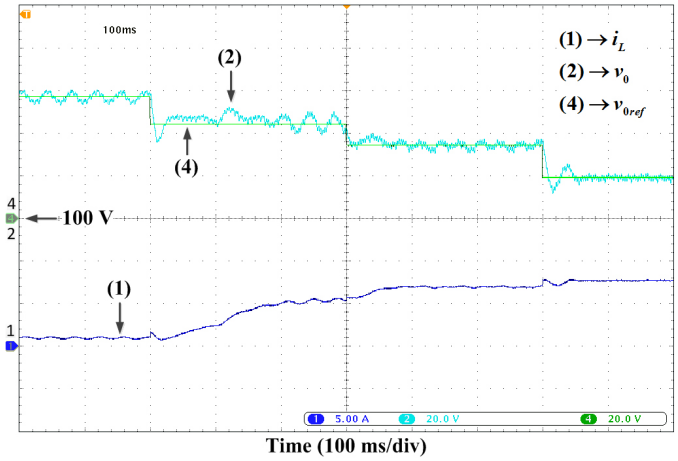

Fig. 16. Voltage and current waveforms in response to upward steps of v_0 under PI controller, and with incorrect value of C_b: v_0(20 V/div), i_L(5 A/div).

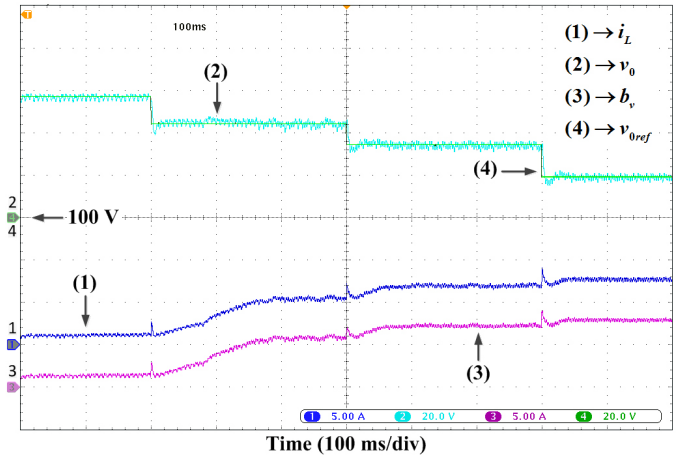

Fig. 17. Voltage and current waveforms in response to upward steps of v_0 under CTMPC, and with incorrect value of C_b: v_0(20 V/div), i_L(5 A/div), and b_v(5 A/div).

E. Evaluation of the Efficiency of the Developed System

This test was conducted to investigate the switching frequency effect on the efficiency η of the dc-dc boost converter. Such an objective is achieved by evaluating the efficiency η, around the maximum power point, for different values of the switching frequency f_{sc}. From the results, it was found that, in the frequency range f_{sc} : 3.125 → 12.5 kHz, the efficiency η remains almost the same and is about 94 %, indicating that the change in the switching frequency does not have a prominent effect on the efficiency. The possible reason is that the dc-dc boost converter uses only one switching device and the existing semiconductor devices are now capable of operating at a high switching frequency without significant switching losses, especially for low power applications. The efficiency of the dc-dc boost converter can be further improved if the power converter module, consisting of the inverter and the boost converter, operates at its nominal power of 20 kVA. This is because the power converter is usually designed to function at high efficiency when it operates at its nominal power, while the maximum power of the PV emulator is limited to 1.6 kW.

VI. Conclusion

In this paper, a robust continuous-time model predictive control has been proposed with the aim of controlling a dc-dc boost converter feeding a grid-connected three-phase inverter by using a cascaded control scheme, as found in many PV applications. The use of continuous-time MPC allows achieving a good tracking performance in response to a smooth reference, whereas the disturbance observer permits to eliminate the steady-state error caused by parametric uncertainty and unknown PV current. Therefore, the composite controller offers excellent transient and steady-state performances throughout the whole operating range. Moreover, the design process was comprehensively described. A PI controller was also designed to control the grid-tied inverter for performance testing of the proposed controller with the consideration of the real dynamics.

Both simulation and experimental results demonstrated the effective control of the dc-dc boost converter to initiate a stable and accurate steady-state regime, while providing a good dynamic performance over the entire operating range.

Appendix A
Parameters of the Complete Solar Energy Conversion System Under Study

The parameters of the grid-tied inverter and the boost converter are v_{dc} = 165 V, L = 6.8 mH, R = 0.1 Ω, C = 1.052 mF, ω = 314.15 rad/s, C_b = 0.16 mF, and L_b = 5 mH. The line-to-line grid voltage is equal to 70 V.

Appendix B
Modelling and Parameters of the Photovoltaic Array

An equivalent circuit of the PV cell, known as a single-diode model, including the series and parallel resistances, is shown in Fig. 18. But, the practical equation that usually adopted to describe the *I–V* characteristic of a PV array is given as follows

$$I = I_{pv} - I_0 \left[\exp\left(\frac{V + R_s I}{V_t a} \right) - 1 \right] - \frac{V + R_s I}{R_p} \qquad (33)$$

where I_{pv}, I_0 and V_t are the PV current, the saturation current, and the thermal voltage, respectively, of the array. Such variables are expressed as functions of the operating

conditions as follows

$$\begin{cases} I_{pv} = \left(I_{pv,n} + K_I\left(T - T_n\right)\right)\dfrac{G}{G_n} \\ I_0 = \dfrac{\left(I_{sc,n} + K_I\left(T - T_n\right)\right)}{\exp\left(\left(V_{oc,n} + K_v\left(T - T_n\right)\right)/aV_t\right) - 1} \\ V_t = \dfrac{N_s K T}{q} \end{cases} \tag{34}$$

where T and G are the actual temperature and irradiation. Here, the temperature measurement is expressed in Kelvin. The rest of the parameters are given in the Table I.

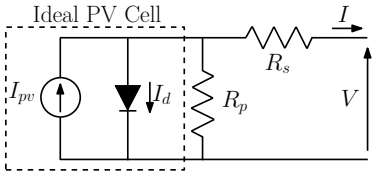

Fig. 18. Equivalent circuit of a single-diode model of a PV cell

TABLE I
PARAMETERS OF THE SIMULATED PV ARRAY AT $T_n = 25\ ^\circ$C AND $G_n = 1000\ W/m^2$

Series Resistance R_s	0.221 Ω
Parallel Resistance R_p	415.405 Ω
Nominal light-generated current $I_{pv,n}$	8.214 A
Nominal short-circuit current $I_{sc,n}$	8.21 A
Short-circuit current/temperature coefficient K_I	0.0032 A/K
Open-circuit voltage/temperature coefficient K_v	-0.1230 V/K
Boltzman constant K	1.3806503×10^{-23} J/K
Nominal temperature in Kelvin T_n	25 °C
Nominal irradiation G_n	1000 W/m^2
Electron charge q	1.60217646×10^{-19} C
Diode ideality constant a	1.3
Nominal open-circuit voltage $V_{oc,n}$	32.9 V
Number of cells connected in series N_s	54

In practical applications, the PV system consists of connecting N_m PV arrays in series to increase the voltage, and N_p PV arrays in parallel to increase the current. In such conditions, the practical equation (33) becomes

$$I = N_p I_{pv} - N_p I_0\left[\exp\left(\frac{V + R_{seq} I}{N_m V_t a}\right) - 1\right] - \frac{V + R_{seq} I}{R_{peq}} \tag{35}$$

where R_{seq}, and R_{peq} are the equivalent resistances, and are determined as follows

$$R_{seq} = R_s\frac{N_m}{N_p}; \quad R_{peq} = R_p\frac{N_m}{N_p} \tag{36}$$

For the purpose of generating the *I–V* characteristic plotted in Fig. 3, it was found that N_m = 4.9 and N_p = 1.02.

REFERENCES

[1] J. Viinamäki, J. Jokipii, T. Messo, T. Suntio, M. Sitbon, and A. Kuperman, "Comprehensive dynamic analysis of photovoltaic generator interfacing dc–dc boost power stage," *IET Renew. Power Gen.*, vol. 9, no. 4, pp. 306–314, 2015.

[2] M. Mahmud, H. Pota, and M. Hossain, "Dynamic stability of three-phase grid-connected photovoltaic system using zero dynamic design approach," *IEEE J. Photovolt.*, vol. 2, no. 4, pp. 564–571, Oct 2012.

[3] C. Y. Tang, Y. T. Chen, and Y. M. Chen, "PV power system with multi-mode operation and low-voltage ride-through capability," *IEEE Trans. Ind Electron.*, vol. 62, no. 12, pp. 7524–7533, Dec 2015.

[4] P. Sharma and V. Agarwal, "Maximum power extraction from a partially shaded PV array using shunt-series compensation," *IEEE J. Photovolt.*, vol. 4, no. 4, pp. 1128–1137, July 2014.

[5] Z. Chen, P. Yang, G. Zhou, J. Xu, and Z. Chen, "Variable duty cycle control for quadratic boost PFC converter," *IEEE Trans. Ind Electron.*, vol. PP, no. 99, pp. 1–1, 2016.

[6] O. Lopez-Santos, L. Martinez-Salamero, G. Garcia, H. Valderrama-Blavi, and T. Sierra-Polanco, "Robust sliding-mode control design for a voltage regulated quadratic boost converter," *IEEE Trans. Power Electron.*, vol. 30, no. 4, pp. 2313–2327, April 2015.

[7] D. Sera, L. Mathe, T. Kerekes, S. V. Spataru, and R. Teodorescu, "On the perturb-and-observe and incremental conductance MPPT methods for PV systems," *IEEE J. Photovolt.*, vol. 3, no. 3, pp. 1070–1078, July 2013.

[8] M. Villalva, T. de Siqueira, and E. Ruppert, "Voltage regulation of photovoltaic arrays: small-signal analysis and control design," *IET Power Electron.*, vol. 3, no. 6, pp. 869–880, 2010.

[9] J. Thongpron, K. Kirtikara, and C. Jivacate, "A method for the determination of dynamic resistance of photovoltaic modules under illumination," *Sol. Energy Mater. Sol. Cells*, vol. 90, no. 18, pp. 3078–3084, 2006.

[10] L. Nousiainen, J. Puukko, A. Mäki, T. Messo, J. Huusari, J. Jokipii, J. Viinamäki, D. Lobera, S. Valkealahti, and T. Suntio, "Photovoltaic generator as an input source for power electronic converters," *IEEE Trans. Power Electron.*, vol. 28, no. 6, pp. 3028–3038, 2013.

[11] A. Urtasun and D. Lu, "Control of a single-switch two-input buck converter for MPPT of two PV strings," *IEEE Trans. Ind. Electron.*, vol. 62, no. 11, pp. 7051–7060, 2015.

[12] A. Urtasun, P. Sanchis, and L. Marroyo, "Adaptive voltage control of the dc/dc boost stage in PV converters with small input capacitor," *IEEE Trans. Power Electron.*, vol. 28, no. 11, pp. 5038–5048, 2013.

[13] M. Sitbon, S. Schacham, and A. Kuperman, "Disturbance observer-based voltage regulation of current-mode-boost-converter-interfaced photovoltaic generator," *IEEE Trans. Ind. Electron.*, vol. 62, no. 9, pp. 5776–5785, 2015.

[14] M. Soroush and C. Kravaris, "A continuous-time formulation of nonlinear model predictive control," *Int. J. Control*, vol. 63, no. 1, pp. 121–146, 1996.

[15] P. J. Gawthrop, H. Demircioglu, and I. I. Siller-Alcala, "Multivariable continuous-time generalised predictive control: A state-space approach to linear and nonlinear systems," in *IEE Proc. Control Theory Appl.*, vol. 145, no. 3. IET, 1998, pp. 241–250.

[16] W.-H. Chen, D. J. Ballance, P. J. Gawthrop, J. J. Gribble, and J. O'Reilly, "Nonlinear PID predictive controller," *IEE Proc. Control Theory Appl.*, vol. 146, no. 6, pp. 603–611, 1999.

[17] J. Yang and W. X. Zheng, "Offset-free nonlinear MPC for mismatched disturbance attenuation with application to a static var compensator," *IEEE Trans. Circuits Sys. II: Express Briefs*, vol. 61, no. 1, pp. 49–53, Jan 2014.

[18] J. Yang, W. Zheng, S. Li, B. Wu, and M. Cheng, "Design of a prediction accuracy enhanced continuous-time MPC for disturbed systems via a disturbance observer," *IEEE Trans. Ind. Electron.*, vol. 62, no. 9, pp. 5807–5816, 2015.

[19] R. Errouissi, M. Ouhrouche, W.-H. Chen, and A. M. Trzynadlowski, "Robust cascaded nonlinear predictive control of a permanent magnet synchronous motor with antiwindup compensator," *IEEE Trans. Ind. Electron.*, vol. 59, no. 8, pp. 3078–3088, 2012.

[20] R. Errouissi, S. M. Muyeen, A. Al-Durra, and S. Leng, "Experimental validation of robust continuous nonlinear model predictive control based grid-interlinked photovoltaic inverter," *IEEE Trans. Ind. Electron.*, DOI: 10.1109/TIE.2015.2508920, 2015.

[21] P. E. Kakosimos, A. G. Kladas, and S. N. Manias, "Fast photovoltaic-system voltage-or current-oriented mppt employing a predictive digital current-controlled converter," *IEEE Trans. Ind. Electron.*, vol. 60, no. 12, pp. 5673–5685, 2013.

[22] E. Mamarelis, G. Petrone, and G. Spagnuolo, "An hybrid digital-analog sliding mode controller for photovoltaic applications," *IEEE Trans. Ind. Info.*, vol. 9, no. 2, pp. 1094–1103, May 2013.

[23] E. Bianconi, J. Calvente, R. Giral, E. Mamarelis, G. Petrone, C. Ramos-Paja, G. Spagnuolo, and M. Vitelli, "A fast current-based MPPT technique employing sliding mode control," *IEEE Trans. Ind. Electron.*, vol. 60, no. 3, pp. 1168–1178, 2013.

[24] M. Goncalves Wanzeller, R. Alves, J. da Fonseca Neto, and W. Fonseca, "Current control loop for tracking of maximum power point supplied for photovoltaic array," *IEEE Trans. Instrum. Measurement*, vol. 53, no. 4, pp. 1304–1310, 2004.

[25] W.-H. Chen, D. J. Ballance, and P. J. Gawthrop, "Optimal control of nonlinear systems: a predictive control approach," *Automatica*, vol. 39, no. 4, pp. 633–641, 2003.
[26] Y. I. Son, I. H. Kim, D. S. Choi, and H. Shim, "Robust cascade control of electric motor drives using dual reduced-order PI observer," *IEEE Trans. Ind. Electron.*, vol. 62, no. 6, pp. 3672–3682, 2015.
[27] D. R. Espinoza-Trejo, E. Barcenas-Barcenas, D. U. Campos-Delgado, and C. H. De Angelo, "Voltage-oriented input–output linearization controller as maximum power point tracking technique for photovoltaic systems," *IEEE Trans. Ind. Electron.*, vol. 62, no. 6, pp. 3499–3507, 2015.
[28] S.-K. Chung, "A phase tracking system for three phase utility interface inverters," *IEEE Trans. Power Electron.*, vol. 15, no. 3, pp. 431–438, 2000.
[29] R. Kadri, J.-P. Gaubert, and G. Champenois, "An improved maximum power point tracking for photovoltaic grid-connected inverter based on voltage-oriented control," *IEEE Trans. Ind. Electron.*, vol. 58, no. 1, pp. 66–75, 2011.
[30] P. Verdelho and G. Marques, "DC voltage control and stability analysis of PWM-voltage-type reversible rectifiers," *IEEE Trans. Ind. Electron.*, vol. 45, no. 2, pp. 263–273, 1998.
[31] M. Villalva, J. Gazoli, and E. Filho, "Comprehensive approach to modeling and simulation of photovoltaic arrays," *IEEE Trans. Power Electron.*, vol. 24, no. 5, pp. 1198–1208, 2009.

Rachid Errouissi (M'15) received the B.Sc. degree in electronics from the Faculty of Sciences and Technology of Mohammedia, Morocco, in 1998; the M.Sc. degree in power electronics from École Mohammadia d'ingénieurs in Rabat, Morocco, in 2001; the double M.Sc. degrees in electrical engineering and in automation and system engineering from University Claude Bernard, Lyon, France, in 2002 and 2004; and the Ph.D. degree in electrical engineering from the University of Quebec, Chicoutimi, QC, Canada, in 2010. From 2011 to 2014, he worked as a Postdoctoral Researcher with the Department of Electrical and Computer Engineering, University of New Brunswick. Since 2014, he has been with the Petroleum Institute, Abu Dhabi, UAE, where he is currently conducting research works in renewable energy and advanced control systems. His area of interests include advanced control, nonlinear control, electric machines and drives, and renewable energy conversion systems. He is a registered Professional Engineer in the province of New Brunswick, Canada.

Ahmed Al-Durra (S'07-M'10-SM14) received the B.S., M.S., and PhD in Electrical and Computer Engineering from the Ohio State University in 2005, 2007, and 2010, respectively. For his M. Sc. degree, he investigated the application of several nonlinear control techniques on automotive traction PEM fuel cell systems. He conducted his PhD research at the Center for Automotive Research in the Ohio State University on the applications of modern estimation and control theories to automotive propulsion systems. At the present, he is an Associate Professor in the Electrical Engineering Department at the Petroleum Institute, Abu Dhabi, UAE. His research interests are application of estimation and control theory in power system stability, Micro and Smart Grids, renewable energy, and process control. He has published over 70 scientific articles in Journals and International Conferences. Dr. Ahmed has successfully accomplished several research projects at international and national levels. He is the co-founder of Renewable Energy Laboratory at the Petroleum Institute, and Senior Member in IEEE.

S. M. Muyeen (S'03-M'08-SM'12) received his B.Sc. Eng. Degree from Rajshahi University of Engineering and Technology (RUET), Bangladesh formerly known as Rajshahi Institute of Technology, in 2000 and M. Sc. Eng. and Dr. Eng. Degrees from Kitami Institute of Technology, Japan, in 2005 and 2008, respectively, all in Electrical and Electronic Engineering. His PhD research work focused on wind farm stabilization from the viewpoint of LVRT and frequency fluctuation. After completing his Ph.D. program he worked as a Postdoctoral Research Fellow under the versatile banner of Japan Society for the Promotion of Science (JSPS) from 2008-2010 at the Kitami Institute of Technology, Japan. At the present, he is working as Associate Professor in Electrical Engineering Department at the Petroleum Institute, Abu Dhabi. His research interests are power system stability and control, electrical machine, FACTS, energy storage system (ESS), Renewable Energy, and HVDC system. He has been a Keynote Speaker and an Invited Speaker at many international conferences, workshops, and universities. He has published over 150 articles in different journals and international conferences. He has published five books as an author or editor. Dr. Muyeen is the senior member of IEEE.